Comparison of Lignin Fractions Isolated from Wheat Straw Using Alkaline and Acidic Deep Eutectic Solvents (DESs)

Xin Yue[a], Terhi Suopajärvi[a], Otto Mankinen[b,c], Marja Mikola[e], Atte Mikkelson[d], Juha Ahola[e], Sami Hiltunen[b], Sanna Komulainen[b], Anu M. Kantola[b], Ville-Veikko Telkki[b], Henrikki Liimatainen[a]*

[a] *Fiber and Particle Engineering Research Unit, University of Oulu, P.O. Box 4300, 90014 Oulu, Finland*

[b] *NMR Research Unit, University of Oulu, P.O.Box 4300, 90014 Oulu, Finland*

[c] *Oulu Functional NeuroImaging Group, Research Unit of Medical Imaging, Physics and Technology, Medical Research Center Oulu, University of Oulu and Oulu University Hospital, P.O.Box 50, 90029 Oulu University Hospital, Finland*

[d] *VTT Technical Research Centre of Finland, Vuorimiehentie 3, 02150 Espoo, Finland*

[e] *Chemical Process Engineering Research Unit, University of Oulu, P.O. Box 4300, 90014 Oulu, Finland*

∗ Corresponding author (Henrikki Liimatainen) at: Fiber and Particle Engineering Research Unit, University of Oulu, P.O. Box 4300, 90014 Oulu, Finland. Tel.: +358 8553 2416; Fax: +358 8553 2405.

ABSTRACT

This study aims to examine the characteristics of two solid lignin fractions isolated from wheat straw using alkaline and acidic deep eutectic solvents (DESs). The chemical properties and morphological characteristics of the two lignin fractions were evaluated by measuring their purity, elemental composition, molecular weight and particle size distributions, and microstructure. Their chemical structure was evaluated using DRIFT spectroscopy, GPC, TGA, ^{13}C NMR, ^{31}P NMR, and HSQC NMR. Our findings showed that the lignin isolated using alkaline DES was less pure and had smaller particle size, higher molecular weight, and thermal stability compared to the lignin isolated using acidic DES. Their lignin structure was also determined to be different due to varying selective fractures on the linkages of lignin. These results suggest that the DES treatments could selectively extract lignin from wheat straw with different yields, composition, morphology, and structure, which could then provide a theoretical basis for the selection of DESs for specially appointed lignin extraction.

Keywords: Wheat straw, Alkaline and acidic DESs, Lignin, Morphological characteristics, Structural features

INTRODUCTION

Wheat straw has been considered as one of the most abundant lignocellulosic agricultural residues in the world, having an annual production of more than 800 million tons globally[1,2]. This residue ends up commonly to open-field burning, landfilling, or incineration[3]. It is rarely used, e.g., in the pulping industry, due to environmental issues and challenges associated with the alkali chemical recovery. Furthermore, current treatments of wheat straw have been reported to cause air pollution as it releases

significant quantities of greenhouse gases, particulates, and smoke, which can pose a direct threat to human health[4].

Similar to other lignocellulosic biomasses, wheat straw is composed of three major components, and these are cellulose (28.8–51.5 %), hemicellulose (10.5–43 %), and lignin (5.4–30 %); trace amounts of extractives and high levels of silica-containing ash (2–15 %) are also noted[5,6]. The composition can vary, all depending on the species, growing regions, and the different fractions of wheat straw. Because of its high carbohydrate content, wheat straw has been considered as a potential resource for ethanol biorefinery. According to the base case model, 0.2 billion liters of denatured ethanol can be produced per year using approximately 900,000 tons per year of wheat straw feedstock[7]. In addition to carbohydrates, wheat straw is also identified as a highly potential source of lignin. However, the lignin derived specifically from wheat straw is still underutilized in high-end applications; however, it can be facilitated by tailoring the characteristics of lignin fraction, which are strongly attributed to the isolation techniques.

Lignin consists a complex class of cross-linked phenolic polymers existing in plant cells[8]. It provides plant cells their strength and hardness, and it has the ability to prevent biological damage and water erosion. It is also known to have antibacterial, anti-oxidative, and flame-retardant properties. In nature, lignin is considered the second largest renewable polymeric bioresource after cellulose and the only non-petroleum resource that can provide notable amount of renewable aromatic compounds. The prerequisite for effective utilization of lignin is its efficient separation from the cellulose and hemicellulose matrix of plant raw materials, including its feasible composition and structural characteristics for further processing. At present, the conventional separation and extraction methods adopted for lignin mainly include alkali treatment[9], acid

hydrolysis/thioacid hydrolysis[10], enzymatic hydrolysis[11], glycerol method[12], ball-milling[13], pyrolysis[14], hydrothermal treatment[15], steam explosion[16], organic solvent extraction[17], ionic liquid extraction[18], etc. However, most of these previously established lignin isolation methods have been associated with disadvantages due to high energy consumption, environmental problems, undesirable alteration of lignin properties, low lignin extraction rate, or high costs.

Recently, a new class of green chemicals, i.e., deep eutectic solvents (DESs), has been harnessed to biomass processing. The DESs have been determined to consist a eutectic mixture formed typically from a quaternary ammonium or metal salt and a hydrogen bond donor. DESs are often considered as a sub-class of ionic liquids; however, compared to traditional ionic liquids, DESs are of advantage due to its simple preparation, high abundance of raw materials, low price, environmental friendliness, and biodegradability. Previous DESs have also been used in the removal of lignin and fractionation of other components from biomasses[19-23]. It has been shown that DESs can be used for efficient lignin removal, in order to obtain a high-quality lignin[24-27]. We previously used six different deep eutectic solvent (DES) treatments—five acidic (natural organic acid–choline chloride) and one alkaline (K_2CO_3–glycerol)—to compare the delignification and nanofibrillation of agricultural by-products[28]. However, the properties of lignin fractions are known to be strongly associated with the chemical characteristics of used solvent systems; furthermore, the characteristics and differences of lignins separated using different DESs remain to be poorly understood. Specifically, there is scarcity on studies examining the fractionation of biomasses using alkaline DESs.

In this work, acidic and alkaline DESs were used in isolating lignin fractions from wheat straw. The separated lignins were characterized by field emission scanning electron

microscopy (FESEM), transmission electron microscopy (TEM), gel permeation chromatography (GPC), diffuse reflectance infrared Fourier transform spectrometry (DRIFT), thermogravimetric analysis (TGA), and nuclear magnetic resonance (NMR) in terms of their physical properties, chemical composition, and structural characteristics in order to provide a relevant research basis for the separation and high-value utilization of lignin.

MATERIALS AND METHODS

Raw materials and chemicals

The wheat straw (Chile) was oven-dried and milled to a particle size of approximately 1 millimeter. The sample initially contained 22.1 wt% lignin, 39.8 wt% cellulose, 18.0 wt% hemicelluloses and ash 4.5 wt%. Choline chloride (99 wt%) was obtained from Algry Quimica, S.L. (Spain), while glycerol (98 wt%), lactic acid (90 wt%), ethanol (96 wt%), and HCl (37 wt%) were purchased from VWR (Finland). Lastly, K_2CO_3 (99 wt%) was obtained from Honeywell (Germany). It should be noted that deionized water was used all throughout the experiments.

Preparation of DES-isolated lignin

Alkaline DES (K_2CO_3-Gly) was prepared by mixing potassium carbonate and glycerol at a molar ratio of 1:5, while acidic DES (Lac-ChCl) was prepared by mixing lactic acid and choline chloride at a molar ratio of 2:1. Mixtures were heated in an oil bath at 100 °C under constant stirring until homogeneous and transparent liquid solution is formed. Approximately 10 g of dry wheat straw (based on the oven-dried mass) was added into the DES, with 15 g of deionized water, and the suspension (3 wt%) was let to stir at 100 °C for 16 h. The reaction was then stopped with the addition of 100 ml ethanol.

117 DES, which contained the dissolved lignin, was separated from the solid fraction by
118 filtration, and deionized water was then added to the mixture to precipitate lignin at room
119 temperature. The alkaline DES filtrate was acidified to pH 3 using HCl before adding
120 deionized water. The precipitated lignin was centrifugated and washed twice with
121 ethanol–water solution (1:10) and dried at 50 °C overnight. The lignin samples extracted
122 by alkaline DES (K_2CO_3-Gly) and acidic DES (Lac-ChCl) were abbreviated as KGL and
123 LCL, respectively. The oven-dried KGL and LCL were used for all quantitative and
124 qualitative analyses performed on this study. Acidic DES supernatant was reused and
125 recycled three times back to the reaction with a new batch of wheat straw. Ethanol was
126 then removed from DES by vacuum rotary evaporation at 40 °C, after which the water
127 was evaporated in an oven at 105 °C for 24 h. The regenerated DES was directly reused
128 for the next wheat straw treatment cycle. These reaction conditions have been described
129 in detail in our previous work[28].

130 **Purity of lignin fractions**

131 ***Klason lignin and acid-soluble lignin***

132 Klason lignin content, i.e., the acid-insoluble lignin from the hydrolysis, was
133 determined gravimetrically using NREL methods[29]. Acid-soluble lignin in the
134 hydrolysate was quantified using ultraviolet spectroscopy (Shimadzu UV-1800, Japan) at
135 215 and 280 nm[30].

136 ***High-performance anion-exchange chromatography (HPAEC)***

137 To determine the carbohydrate and lignin composition, the lignin samples were
138 hydrolyzed using sulfuric acid, and the concentration of monosaccharides was determined
139 using HPAEC with pulse amperometric detection (Dionex ICS-5000 equipped with a
140 CarboPac PA20 column). The polysaccharide content in the samples was then calculated

141 from the corresponding monosaccharides using an anhydro correction of 0.88 for
142 pentoses and 0.9 for hexoses[31]. Approximately 100 mg of each sample was weighted into
143 a hydrolysis tube, 1 ml of 72 wt% sulfuric acid was then added, and samples were pre-
144 hydrolyzed at 30 °C in water bath for 1 h. Then, samples were transferred into a 50 ml
145 volumetric flask, with the addition of 28 ml ultra-pure water. Flasks were sealed with
146 aluminum foil and autoclaved for 60 min at 120 °C. After hydrolysis, the samples were
147 cooled and filtered using 0.45 μm GHP filters. The hydrolysis was performed as five
148 replicate analyses. Hydrolyzed samples were diluted 50-fold using ultra-pure water, and
149 internal standard (deoxy-glucose for monosaccharide and fucose for uronic acid analysis)
150 was added for HPAEC analysis.

151 **Elemental and X-ray photoelectron spectroscopy (XPS) analyses**

152 ***Elemental analysis***

153 An elemental analyzer (CHNS/O FLASH 2000 Series) was used to determine the
154 contents of C, H, N, and S. The samples were weighted in tin capsules, placed inside an
155 auto-sampler, and then dropped into a reactor, which was kept at 960 °C. At this high
156 temperature, organic compounds were converted into elemental gases, which, after
157 reduction, were separated in a chromatographic column and detected using thermal
158 conductivity detector (TCD). The content of O was determined via pyrolysis using silver
159 capsules in the same analyzer. Results were calculated via Certified Elemental
160 Microanalysis standards using K factor (CHNS/CHNS-O Standards Kit: Cystine,
161 Sulphanilamide, Methionine and BBOT: Catalogue Code. Thermo: 33840010).

162 ***XPS analysis***

163 The elemental and chemical data of lignin samples were provided using a Thermo
164 Fisher Scientific ESCALAB 250Xi, equipped with a monochromatized Al Kα x-ray

source (1486.68 eV) operated at 300 W. An electron flood gun with ion bombarding was used for charge compensation. Samples were then pressed on the indium film and analyzed in a high vacuum chamber pressure at 5×10^{-9} mbar. An analyzer pass energy of 20 eV and 150 eV and a step size of 0.1 eV and 1 eV per step were utilized to obtain the high- and low-resolution spectra, respectively. The composition of the surface region (< 5 nm) was determined based on the ratio of the peak areas corrected by the sensitivity factors of the corresponding elements. Due to sample charging, the spectra were corrected using the C 1s hydrocarbon component at 284.8 eV. Avantage Software (UK) was utilized in processing the data. Quantitative analysis of each element was calculated from the peak areas.

Molecular weight distribution and particle size distribution

GPC analysis

The molecular weight distribution of lignin samples was measured using gel permeation chromatography. Agilent 1260 series chromatograph equipped with Phenogel 5 µm 10^4 Å, Phenogel 5 µm 10^3 Å, and Phenogel 5 µm 50 Å columns (Phenomenex) was utilized. Dimethylformamide with 0.05 wt% of LiBr was also used as a mobile phase with a flow rate of 0.5 ml/min. The columns were operated at 35 °C. Detection was carried out using a variable wavelength detector at wavelength 280 nm. The calibration was then conducted with polyethylene glycol/oxide standards (EasyVials PEO/PEG, Agilent Technologies), which were detected using refractive index detector. For the measurements, lignin samples were dissolved in dimethylformamide containing 0.05 wt% of LiBr. Lignin concentrations of the measured samples were of 1 g/L.

Before sampling, lignin samples were acetylated[32]. In brief, lignin (40 mg) was dissolved in a 1:1 (v:v) acetic anhydride/pyridine mixture (2 ml). The reaction was carried

189 out under nitrogen atmosphere at 50 °C for 24 h. Precipitated acetylated DES-lignins were
190 then obtained by adding ethyl ether (200 ml), followed by centrifugation. The precipitate
191 was then washed thrice with ethanol and twice with ethyl ether to ensure the complete
192 removal of acetic acid and pyridine from samples and then dried at 40 °C.

193 ***Particle size analysis***

194 The particle size and size distribution of lignin samples were determined using a
195 laser diffraction particle size analyzer (LS 13 320, Beckman Coulter, Brea, CA, USA).
196 Before measuring, each lignin sample was dispersed in deionized water under ultrasound
197 for 6 min. The mean diameters of samples were then calculated from three replicate
198 measurements.

199 **FESEM and TEM**

200 The visual appearance of the lignin particles was characterized by combining
201 FESEM and TEM. Generally, FESEM provides information on the sample surface and its
202 shape, while TEM provides information on the internal structure of the samples, such as
203 crystal structure, morphology, and stress state.

204 The surface features of lignin samples were obtained using a field emission scanning
205 electron microscopy (Zeiss Sigma HD VP, Oberkochen, Germany) at 5 kV acceleration
206 voltage. All samples were then sputter coated with 5-nm-thick platinum, prior to imaging.
207 The Feret's diameter of lignin particles was calculated using ImageJ software. The
208 morphological characteristics of lignin samples were also analyzed with transmission
209 electron microscope using the JEOL JEM-2200FS (JEOL Ltd., Tokyo, Japan). Around 7
210 μL (0.001 wt% in water) of diluted sample solutions was dropped on top of a carbon-
211 coated copper grid and was further air-dried at room temperature. The high-resolution
212 images were observed using a Quemesa CCD camera with 200 kV accelerating voltage.

213 **DRIFT**

214 The chemical features of lignin samples were analyzed using a Bruker Vertex 80v
215 spectrometer (USA) at room temperature. Around 40 scans per spectra were recorded in
216 a diffuse mode from 600 to 4000 cm^{-1} at a resolution of 2 cm^{-1}. The background was also
217 collected and removed from the measurements prior to analysis.

218 **TGA**

219 The thermal stabilities of lignin samples were determined using a thermogravimetric
220 analyzer (Netzsch STA 449F3, Germany) under nitrogen with a constant rate of 60 ml/min.
221 Approximately 5 mg of each oven-dried sample was carried by an aluminum oxide pan
222 and was further heated from room temperature to 800 °C, with a heating rate at 10 °C/min.

223 **NMR analysis**

224 ***^{13}C nuclear magnetic resonance (^{13}C-NMR)***

225 The DES-lignins (100 mg) were dissolved in 0.6 ml of DMSO-d6 at 25 °C. A total
226 of 40 µl of chromium (III) acetylacetonate (0.01 M) was added to facilitate the relaxation
227 of magnetization. ^{13}C-NMR experiments were carried out on 14.1 T Bruker Avance III
228 600 spectrometer, which was equipped with a 5-mm broadband (BB) probe operating at
229 150.9 MHz for carbon. Experiments were conducted at room temperature, and the
230 positions of the peaks were referenced to the residual solvent peak of DMSO-d6 at 39.52
231 ppm. ^{13}C spectra were then recorded using inverse gated proton decoupling sequence
232 (Bruker standard sequence "zgig30"). ^{13}C-NMR spectra were obtained using a 36 kHz
233 (239 ppm) spectral width, 66k data points, and 21000 scans with a 30-degree tip angle.
234 Measured FIDs were processed via 10 Hz line broadening. Other necessary parameters
235 were optimized to ensure a flat baseline, and, if needed, baseline was corrected before
236 analysis. Relaxation delay was set to at least five times the longest spin-lattice relaxation

237 time (T_1).

238 ***^{31}P nuclear magnetic resonance (^{31}P-NMR)***

239 The quantitative ^{31}P-NMR spectra of lignin samples were collected as described
240 previously[33]. A total of 500 μL of the solvent mixture solution composed of
241 pyridine/deuterated chloroform (1.6:1, v:v) was prepared. The solvent solution was then
242 used to prepare the internal standard solution containing 20.5 mg/ml of cyclohexanol and
243 relaxation reagent consisting of 5.6 mg/ml of chromium (III) acetylacetonate. A total of
244 20 mg of each lignin sample was dissolved in 200 μL pyridine/deuterated chloroform
245 solvent solution, which has been previously prepared. Around 100 μL of the cyclohexanol
246 solution and 100 μL of the chromium (III) acetylacetonate solution were added
247 respectively, followed by 100 μL 2-chloro-4,4,5,5-tetramethyl-1,3,2-dioxaphospholane
248 reagent and then left under ultrasound until lignin has completely dissolved. The 500 μL
249 mixture solution was transferred into NMR tubes for subsequent determination. The
250 quantitative ^{31}P-NMR experiments were performed on 9.4 T Bruker Avance III 400
251 spectrometer equipped with a 5 mm BB probe operating at 162 MHz, and the ^{31}P spectra
252 were recorded with inverse gated proton decoupling sequence with a full 90-degree tip
253 angle at room temperature. The final spectra were recorded with 100 ppm spectral width
254 (16 kHz) and were centered close to an interesting region that lies roughly in between 130
255 ppm and 160 ppm. A total of 6000 scans were acquired and 66k points collected. Sharp
256 peak arising from cyclohexanol peak signal was observed at 144 ppm, which can be used
257 as a reference for other assignments. Compared to previous literature, the spectra are
258 shifted by roughly 1 ppm to upfield. For more precise quantification of hydroxyl groups,
259 deconvolution of each peak was performed.

260 ***Two-dimensional heteronuclear single quantum coherence nuclear magnetic***

resonance (HSQC NMR)

The DES-lignins (100 mg) were dissolved in 0.6 ml of DMSO-d6 at 25 °C. A total of 40 μl of chromium (III) acetylacetonate (0.01 M) was added in order to facilitate the relaxation of magnetization. HSQC NMR experiments were performed on 9.4 T Bruker Avance III 400 spectrometer, equipped with a 5 mm BB probe operating at 400 MHz. Sufficient amounts of dummy scans were applied in order to reach a steady state and avoid sample heating during the experiment at room temperature. Data consisting 4096 by 256 points were then collected. Spectral widths were determined to be 12 ppm for ^{1}H (centered at 4.7 ppm) and 200 ppm for ^{13}C (centered at 100 ppm).

RESULTS AND DISCUSSION

Chemical composition and purity of the lignin fractions

Lignin fractions consisting of solid, brownish particles were obtained from the wheat straw using alkaline and acid DES treatments. The original wheat straw was determined to contain 22.1 wt% of lignin, 39.8 wt% of glucans, 18.0 wt% of xylans, and 4.5 wt% of ash[28]. The contents of Klason lignin (acid-insoluble lignin, AIL) and acid-soluble lignin (ASL) and ash content of separated lignin fractions are summarized in Table 1. The total lignin content and purity of lignin fraction (KGL, 74.8 %) from alkaline treatment was found to be obviously lower than that (LCL, 83.5 %) from acidic treatment in the used conditions. However, the yield of KGL (7.8 %) was higher than that of LCL (6.1 %), presumably due to high ash content of alkaline lignin. In addition, KGL contained more carbohydrates than LCL, with the overall carbohydrate content being still relatively low (< 3.5 wt%) and being mainly derived from sugars associated with hemicelluloses (D-xylose, L-arabinose, and L-galactose)[34]. These carbohydrates are likely attributed to lignin-carbohydrate complexes (LCC), which were determined to hardly cleave during

DES treatment under the described conditions. The typical lignin products (e.g., diluted acid lignin, steam explosion lignin, mechanical milling lignin) obtained, e.g., from the papermaking industry, always contain a significant amount of residual carbohydrates or process chemicals. In traditional alkaline cooking of grasses, SiO_2 usually exists in black liquor in the form of Na_2SiO_3. Similarly, the high ash content of KGL was associated with alkaline-soluble silicates, which exist inherently in the wheat straw biomass[35-37].

Elemental analysis and XPS analysis

The elemental composition of the lignin fractions is presented in Table 2. The lignin samples mainly consisted C and O, and only a small amount of N and negligible amount of S were detected. Because the elemental analyzer converts organic compounds into elemental gases, the main inorganics attributed to residual ash, especially that of SiO_2 in the KGL, was not detected, leading to the obvious lower total element content of KGL compared with that of LCL. The presence of trace nitrogen indicated that some protein or other nitrogen impurities were present in both lignin fractions. The slightly higher N content observed in the LCL can be likely attributed to the choline chloride used in the DES.

Quantitative X-ray photoelectron spectroscopy (XPS) was determined to have the ability to effectively determine the surface composition of lignin samples and changes in the elemental composition, and it provides information about the chemical linkages. The results of elemental compositions calculated from XPS of KGL and LCL are summarized in Table 2. The O/C value commonly shows the proportional amount of lignin, and the O/C ratio of lignin varies from 0.25 to 0.40, depending on the raw material and the separation method used[38]. The ratio of the atomic concentration of O/C was calculated to be at 0.46 for KGL and 0.34 for LCL, respectively. Obviously, the O/C ratio of the LCL

was closer to the theoretical O/C value of pure lignin (O/C = 0.33)[39], which revealed a high purity of LCL lignin and was confirmed also with the results of carbohydrate content analysis (Table 1). Presumably, the high SiO_2 content of KGL has increased its O/C ratio. Consistently, the amount of Si in KGL sample was much higher than that in LCL sample (Table 2), and this was in good agreement with the purity analysis (Table 1). It has previously been reported that silicon co-precipitate under alkaline conditions with lignin oligomers and polymers rather randomly[40].

The fitting data of the core level of C 1s and O 1s spectra peak areas of the KGL and LCL samples are shown in Figure 1, and the relative surface functional group compositions based on the binding energies of C 1s and O 1s single peaks are listed in Table 3. The binding energy distributions are based on previous reports[38,41]. The analysis of these spectra clearly illustrates some significant changes in the chemical structure of lignins from the acidic and alkaline DES treatments. LCL was determined to consist higher amount of groups associated with C−O−C, C−OH, Ph=O, Ph−C=O, and O−O, while KCL was reportedly rich in groups associated with C−C, C−H, Ph−OH, and C−O. The results have confirmed good correlation with the structures of isolated lignins and residual carbohydrates[38,40].

Molecular weight and particle size distributions

The average molecular weight distribution curves of KGL and LCL are presented in Figure 2a. The weight-average (Mw) and number-average (Mn) molecular weights and the polydispersity indexes (PDI, Mw/Mn) of DES-lignin samples calculated from their chromatograms are summarized in Table 4. The PDI of KGL (4.08) was determined to be higher than that of LCL (3.09), which indicated that the molecular weight of KGL was more heterogeneous. Both the weight- and number-average molecular weights of KGL

were higher than that of LCL (Table 4), revealing more effective depolymerization and fragmentation of macromolecular structure of lignin under acidic conditions. The results also indicated that LCL had a lower molecular weight compared to MWL, alkaline, and acetic acid lignin[42]. In addition, both KGL and LCL showed higher molecular weight dispersion (PDI). It has previously been suggested that the cleavage of ether linkages in the acidic DES plays an important role in the depolymerization of lignin, which promoted its separation from biomass[24]. Overall, DESs have provided a mild acidic and alkaline medium to facilitate the cleavage of unstable ether linkages, resulting in the formation of low molecular weight lignin fragments[43].

As indicated in Figure 2b, both lignin fractions consisted of microparticles. The mean diameter of KGL lignin particles was approximately 2.83 μm, while the LCL consisted of particles having the mean diameter of around 4.25 μm. In general, the LCL fractions consisted of larger and more aggregated particles than those of KGL fraction. Both samples had a broad particle size distribution, which clearly indicated the diversity of aggregation during the precipitation process.

Visual appearance of the lignin particles

In order to elucidate the effect of alkaline and acidic DES treatments on the morphology of lignin particles, the lignin samples were analyzed using FESEM and TEM, as shown in Figure 3 (a–d). Both lignin fractions showed a hierarchical sub-structure, but the surface morphology of KGL and LCL was deemed quite different. The surface of KGL sample was found to be extraordinarily rough in the micron-scale, while the surface of LCL sample was much more uniform and moderately smooth (Figures 3a and b). It was obvious that the particles of both KGL and LCL consisted of small nano-sized entities, which were all aggregated together; however, the size of individual particle of KGL was

found to be greatly larger than that of LCL, as presented in Figures 3c and d. The KGL particle size ranged from 70 nm to 110 nm in Feret's diameter, while LCL particles' diameter ranged from 35 nm to 65 nm. The size of lignin particles might have been affected by many factors, such as the isolation processes, the purity of lignin, and the surface charge of particles. The anionic charges of KGL and LCL were 0.266 and 0.036 meq/g, respectively, which were detected using polyelectrolyte titration (Mütek PCD 03). However, even though the surface charges of the two lignin particles were quite different, whether it is the main factor affecting the size of the lignin particles has not yet been determined.

The TEM images (Figures 3e and f) revealed that the KGL and LCL particles were roughly spherical, but almost indistinguishable because they appeared to melt together. The aggregation and coalescence were due to the formation of solid bridges connecting the lignin particle groups as the lignin particles contained or were in contact with a small amount of the solvent[41].

TGA of the lignin fractions

The TG and DTG (the first derivative of TG, representing the corresponding weight loss rate) curves of KGL and LCL are shown in Figure 4a. The data of raw material (wheat straw) is also shown for comparison. Overall, the continuous pyrolysis of lignin was observed at broad temperature range of 130–780 °C. The TGA curves of both lignin samples have presented similar three-stage thermal decomposition processes despite their different characteristics. The minor weight loss from room temperature to 150 °C was mainly due to the evaporation of water, including free and bound water, and partly from the dehydration reaction[44]. This indicated that the two lignin samples, KGL and LCL, had almost the same properties in the first pyrolysis stage.

The second, more pronounced, pyrolysis stage appeared between 150 °C and 480 °C, and it was likely ascribed to the degradation of carbohydrates, phenols, alcohols, and aldehydes into CO, CO_2, and CH_4[43]. At this stage, the maximum weight loss rate of LCL was 0.27 %/min at around 252 °C and 0.25 %/min at approximately 357 °C, respectively. The highest weight loss rate of KGL was 0.17 %/min at 249 °C and 0.21 %/min at 327 °C, respectively. These results indicated that KGL was determined to be more stable than LCL over this temperature range. The first notable peak of weight loss rate of LCL was slightly narrower than that of KGL, which suggested that the weight loss rate of the former was faster. This might be attributed to lower molecular weight of LCL, which was consistent with the molecular weight analysis results (Table 4 and Figure 2a).

The third, and slower, pyrolysis stage occurred after 480 °C. Here, both lignins had almost identical mass loss rate. Both lignins resulted in a notable amount of ash residue, accounting for about 45 wt% of KGL and 35 wt% of LCL, respectively. The higher ash content of KGL was determined to be related to high silicon amount as confirmed also by elemental analysis and XPS results (Table 2).

By contrast, the thermal decomposition of wheat straw also occurred in three weight loss steps. The first weight loss step corresponding to the remove of the moisture of wheat straw occurred from room temperature to 200 °C. The second weight loss step occurred at the temperature range between 200 and 400 °C, which was significantly faster than the pyrolysis of KGL and LCL. This is because wheat straw contains the more easily pyrolyzed extractives, cellulose and hemicellulose compared with KGL and LCL. The third weight loss step of wheat straw observed after 400 °C is similar to the pyrolysis of KGL and LCL. This step corresponds to the pyrolysis of lignin and charring of the residue.

The amount of ash residue from wheat straw was 35 wt%, which was similar to the content from LCL but significantly less than that from KGL.

DRIFT and NMR analysis of lignin fractions

DRIFT was used to demonstrate the structural differences in the functional groups of lignin isolated by DES treatments. The characteristic peaks of KGL and LCL in the region of 400–4000 cm^{-1} are shown in Figure 4b. The data of raw material (wheat straw) is also shown for comparison. Band shapes of both KGL and LCL spectra had substantially similar general appearance, except for some insignificant shifts of some peaks, indicating only minor differences in the backbone structure of lignins. However, the peak intensities of many bands have altered. A wide absorption band appearing at 3428 cm^{-1} was ascribed to the stretching vibration of O–H from aromatic or aliphatic structure. The typical characteristic bands appearing at 1604 cm^{-1}, 1513 cm^{-1}, and 1425 cm^{-1} were attributed to the vibrations of the phenylpropane skeleton. In addition, the vibrations of the alkane C–H at 2925 cm^{-1} and 1463 cm^{-1} were observable, and an intense absorption band at 2852 cm^{-1} was assigned to methoxyl C–H deformation stretching. All those bands have presented the typical signal pattern expected for lignin structure[45]. In contrast, the DRIFT of wheat straw cannot provide additional information due to the heterogeneous structures of different components.

The strong absorption at 1711 cm^{-1} of KGL and 1739 cm^{-1} of LCL arose from the carbonyl group associated with non-conjugated ketone and carboxyl group stretching, while the subdued absorption at 1656 cm^{-1} indicated conjugated carbonyl. It has been reported that the β–O–4 cleavage results in Hibbert's ketone under acidic conditions.[46-49] This is supported by the fact that a large number of non-conjugated carbonyl groups attributed to the formation of Hibbert's ketone in the acidic DES treatment were detected

in LCL by DRIFT. This result was further confirmed in the subsequent NMR analyses, which proved that the β–O–4 bonds were cleaved during acidic DES treatment. A stronger peak of LCL associated with non-conjugated groups suggested that acidic DES promoted more breakage of β–O–4 bonds compared with alkaline DES. Moreover, the peaks intensity associated with phenolic and primary aliphatic OH groups of lignin, at 1367 cm^{-1} and 1049 cm^{-1}, respectively, were stronger with LCL. These results indicate that the content of phenolic and primary aliphatic OH groups in LCL was higher than that in KGL. The higher content of phenolic OH groups in LCL was due to the cleavage of β–O–4 bond caused by acidic DES treatment. The formation of Hibbert's ketone detected by subsequent NMR analysis also proved this result. The content of primary aliphatic OH groups in KGL was lower than that in LCL, which was due to the loss of primary aliphatic OH groups caused by alkaline DES treatment. This is a similar effect that is noted in the soda pulping.[45]

The chemical structure of KGL and LCL was further analyzed using quantitative ^{13}C, ^{31}P and HSQC NMR. The ^{13}C and ^{31}P NMR spectra of the lignin samples are shown in Figures 5 and 6, respectively. Summary of the major structural parameters are presented in Table 5. The signals between 71 and 83 ppm correspond to the spectral region of Cα and Cβ in β–O–4 in the ^{13}C NMR spectra. The signals of KGL were much stronger than that of LCL, suggesting a large amount of ether linkages present in KGL. This result was also supported by the DRIFT analysis, indicating more pronounced cleavage of β–O–4 bond with acidic DES treatment in LCL. In addition, the amount of primary (60–68 ppm in ^{13}C NMR spectra) aliphatic hydroxyl group was higher in LCL than that of KGL. However, the number of secondary (72–75 ppm in ^{13}C NMR spectra) aliphatic hydroxyl groups in LCL was as expected smaller than that of KGL, which was also confirmed by

DRIFT.

The quantitative ^{31}P NMR spectra of lignin samples (Figure 6) show the signals of various hydroxyl groups. Generally, the main hydroxyl groups present in lignin are the aliphatic hydroxyls. The data of ^{31}P NMR (Table 5) shows that both KGL and LCL had the following order of hydroxyl contents: aliphatic OH > phenolic OH > carboxylic OH. The major phenolic hydroxyls in both KGL and LCL appeared to be C_5 substituted and guaiacyl OH. Syringyl OH and *p*-hydroxyphenyl OH were also detected in both lignins in large amount, which is consistent with the general characteristics of wheat straw lignin. Another striking observation is the higher phenolic hydroxyls in LCL compared to KGL, which confirms the more pronounced cleavage of ether linkages during acidic DES treatment.

To better understand the differences between alkaline and acidic DES treatments, HSQC NMR was conducted to check on the structural characteristics of KGL and LCL. Lignin has been identified as a polymer assembled by phenylpropane units linked by ether (C–O–C) and carbon-carbon (C–C) bonds, which make up its complex entity. The characteristic linkages between phenylpropane units are listed in Figure 7. As expected, the LCL possessed only minor amount of the β–O–4 ether linkages (A), which are found to be abundant in the intact, natural lignin. This finding also confirmed the cleavage of ether linkages as also proven by DRIFT, ^{13}C NMR, and ^{31}P NMR. The HSQC NMR spectra in Figure 7 also illustrated that carbon-carbon (C–C) bonds such as the β–5 (B) and β–β (C) linkages remained the predominant interunit linkages in both KGL and LCL. Appreciable amount of Hibbert's ketone was also detected in LCL, which further verified the cleavage of β–O–4 linkages by acidic DES treatment. Overall, the analyses suggested that the reaction mechanism of acidic degradation of lignin in DES was similar to lignin

acidolysis catalyzed by HCl[46-49]. These results confirmed that acidic DES treatment can potentially be harnessed to selectively cleave ether bonds and relatively little affect the C–C linkages, which is quite different from alkaline DES treatment. However, the precise mechanism behind lignin degradation in the DES requires further investigation.

To summarize, KGL and LCL presented different lignin compositions and average molecular weight distributions. The lower average molecular weight of LCL was associated with the promoted depolymerization of lignin in the acidic DES treatment and was further confirmed by DRIFT, ^{13}C NMR, and HSQC NMR spectra. In addition, an appreciable amount of Hibbert's ketone was detected in LCL using HSQC NMR, indicating that the degradation of lignin in the acidic DES followed similar reaction mechanism to lignin acidolysis. The KGL had lower particle size and higher thermal stability than that of LCL. The visualization of the lignin particles showed also differences between KGL and LCL lignins. The differences in morphology and structure provide a theoretical basis for the respective high-value applications of lignin fractions. For example, KGL with a small particle size and high surface might be used as an efficient absorbent, while the LCL with a lower molecular weight might have more potential for the synthesis of soluble derivatives.

DECLARATION OF COMPETING INTEREST

The authors declare no conflict of interest.

ACKNOWLEDGMENTS

The authors acknowledge the financial support of the ERANet-LAC and Academy of Finland, project: Towards a novel and sustainable biorefinery concept based on green technologies for main commercial grain crop residues (BIOCODE) (No. 311974). The facilities of the Center of Microscopy and Nanotechnology of the University of Oulu were

utilized in this research. Xin Yue thanks China Scholarship Council (CSC) for the financial support. Ville-Veikko Telkki thanks Academy of Finland (grant numbers 289649, 294027 and 319216) and the Kvantum institute (University of Oulu) for the financial support.

REFERENCES

(1) Bentsen, N. S.; Felby, C.; Thorsen, B. J. Agricultural residue production and potentials for energy and materials services. *Prog. Energy Combust. Sci.* **2014**, *40*, 59–73. https://doi.org/10.1016/j.pecs.2013.09.003.

(2) Saha, B. C.; Nichols, N. N.; Qureshi, N.; Kennedy, G. J.; Iten, L. B.; Cotta, M. A. Pilot scale conversion of wheat straw to ethanol via simultaneous saccharification and fermentation. *Bioresour. Technol.* **2015**, *175*, 17–22. https://doi.org/10.1016/j.biortech.2014.10.060.

(3) Bhiday, M. R. Earthworms in agriculture. *Indian Farming* **1994**, *43* (12), 31–34.

(4) Jain, N.; Bhatia, A.; Pathak, H. Emission of air Pollutants from crop residue burning in india. *Aerosol Air Qual. Res.* **2014**, *14* (1), 422–430. https://doi.org/10.4209/aaqr.2013.01.0031.

(5) Adapa, P.; Tabil, L.; Schoenau, G. Compaction characteristics of barley, canola, oat and wheat straw. *Biosyst. Eng.* **2009**, *104* (3), 335–344. https://doi.org/10.1016/j.biosystemseng.2009.06.022.

(6) Ramesh, D.; Muniraj, I.K.; Thangavelu, K.; Karthikeyan, S. Chemicals and fuels production from agro esidues: a biorefinery approach. *Sustainable Approaches for Biofuels Production Technologies* **2019**, *7*, 47–71. https://doi.org/10.1007/978-3-319-94797-6_3

(7) Leistritz, F. L.; Senechal, D. M.; Stowers, M. D.; McDonald, W. F.; Saffron, C. M.; Hodur, N. M. Preliminary feasibility analysis for an integrated biomaterials and ethanol biorefinery using wheat straw feedstock. *AgEcon Search.* **2006**, *1*, 1–48. https://doi.org/10.22004/AG.ECON.23500

(8) Lebo, S. E.; Gargulak, J. D.; McNally, T. J. Lignin. In *Kirk-othmer encyclopedia of chemical technology*; John Wiley & Sons, Inc., Ed.; John Wiley & Sons, Inc.: Hoboken, NJ, USA, 2001; p 12090714120914.a01.pub2. https://doi.org/10.1002/0471238961.12090714120914.a01.pub2.

(9) Wallberg, O.; Jönsson, A.-S.; Wimmerstedt, R. Fractionation and concentration of kraft black liquor lignin with ultrafiltration. *Desalination* **2003**, *154* (2), 187–199. https://doi.org/10.1016/S0011-9164(03)80019-X.

(10) Matsushita, Y.; Yasuda, S. Preparation of anion-exchange resins from pine sulfuric acid lignin, One of the acid hydrolysis lignins. *J. Wood Sci.* **2003**, *49* (5), 423–429. https://doi.org/10.1007/s10086-002-0489-3.

(11) Hu, Z.; Yeh, T.-F.; Chang, H.; Matsumoto, Y.; Kadla, J. F. Elucidation of the structure of cellulolytic enzyme lignin. *Holzforschung* **2006**, *60* (4), 389–397. https://doi.org/10.1515/HF.2006.061.

(12) Hintz, R. W.; Mertens, D. R.; Albrecht, K. A. Effects of sodium sulfite on recovery and composition of detergent fiber and lignin. *J. AOAC Int.* **1996**, *79* (1), 16–22.

(13) Sun, R.; Xiao, B.; Lawther, J. M. Fractional and structural characterization of ball-milled and enzyme lignins from wheat straw. *J. Appl. Polym. Sci.* **1998***, 68,* 1633–1641. https://doi.org/10.1002/(SICI)1097-4628(19980606)68:10<1633::AID-APP12>3.0.CO;2-Y

(14) Alves, A.; Schwanninger, M.; Pereira, H.; Rodrigues, J. Analytical pyrolysis as a direct method to determine the lignin content in wood. *J. Anal. Appl. Pyrolysis* **2006**, *76* (1–2), 209–213. https://doi.org/10.1016/j.jaap.2005.11.004.

(15) Kang, S.; Xiao, L.; Meng, L.; Zhang, X.; Sun, R. Isolation and structural characterization of lignin from cotton stalk treated in an ammonia hydrothermal system. *IJMS* **2012**, *13* (12), 15209–15226. https://doi.org/10.3390/ijms131115209.

(16) Li, J.; Gellerstedt, G.; Toven, K. Steam explosion lignins; their extraction, structure and potential as feedstock for biodiesel and chemicals. *Bioresour. Technol.* **2009**, *100* (9), 2556–2561. https://doi.org/10.1016/j.biortech.2008.12.004.

(17) Cybulska, I.; Brudecki, G.; Rosentrater, K.; Julson, J. L.; Lei, H. Comparative study of organosolv lignin extracted from prairie cordgrass, switchgrass and corn stover. *Bioresour. Technol.* **2012**, *118*, 30–36. https://doi.org/10.1016/j.biortech.2012.05.073.

(18) Kim, J.-Y.; Shin, E.-J.; Eom, I.-Y.; Won, K.; Kim, Y. H.; Choi, D.; Choi, I.-G.; Choi, J. W. Structural features of lignin macromolecules extracted with ionic liquid from poplar wood. *Bioresour. Technol.* **2011**, *102* (19), 9020–9025. https://doi.org/10.1016/j.biortech.2011.07.081.

(19) Francisco, M.; van den Bruinhorst, A.; Kroon, M. C. New natural and renewable low transition temperature mixtures (LTTMs): Screening as solvents for lignocellulosic biomass processing. *Green Chem.* **2012**, *14* (8), 2153. https://doi.org/10.1039/c2gc35660k.

(20) Hong, S.; Sun, X.; Lian, H.; Pojman, J. A.; Mota-Morales, J. D. Zinc chloride/acetamide deep eutectic solvent-mediated fractionation of lignin produces high- and low-molecular-weight fillers for phenol-formaldehyde resins. *J. Appl. Polym. Sci.* **2020**, *137* (7), 48385. https://doi.org/10.1002/app.48385.

(21) Lian, H.; Hong, S.; Carranza, A.; Mota-Morales, J. D.; Pojman, J. A. Processing of lignin in urea–zinc chloride deep-eutectic solvent and its use as a filler in a phenol-formaldehyde resin. *RSC Adv.* **2015**, *5* (36), 28778–28785. https://doi.org/10.1039/C4RA16734A.

(22) Pena-Pereira, F.; Namieśnik, J. Ionic liquids and deep eutectic mixtures: Sustainable solvents for extraction processes. *ChemSusChem* **2014**, *7* (7), 1784–1800. https://doi.org/10.1002/cssc.201301192.

(23) Zainal-Abidin, M. H.; Hayyan, M.; Hayyan, A.; Jayakumar, N. S. New horizons in the extraction of bioactive compounds using deep eutectic solvents: A review. *Anal. Chim. Acta* **2017**, *979*, 1–23. https://doi.org/10.1016/j.aca.2017.05.012.

(24) Alvarez-Vasco, C.; Ma, R.; Quintero, M.; Guo, M.; Geleynse, S.; Ramasamy, K. K.; Wolcott, M.; Zhang, X. Unique low-molecular-weight lignin with high purity extracted from wood by deep eutectic solvents (DES): A source of lignin for valorization. *Green Chem.* **2016**, *18* (19), 5133–5141. https://doi.org/10.1039/C6GC01007E.

(25) Li, T.; Lyu, G.; Liu, Y.; Lou, R.; Lucia, A. L.; Yang, G.; Chen, J.; Saeed, A. M. H. Deep eutectic solvents (DESs) for the isolation of willow lignin (salix matsudana cv. zhuliu). *Int. J. Mol. Sci.*

2017, *18* (11), 1–11. https://doi.org/10.3390/ijms18112266.

(26) Malaeke, H.; Housaindokht, M. R.; Monhemi, H.; Izadyar, M. Deep eutectic solvent as an efficient molecular liquid for lignin solubilization and wood delignification. *J. Mol. Liq.* **2018**, *263*, 193–199. https://doi.org/10.1016/j.molliq.2018.05.001.

(27) Yang, R.; Cao, Q.; Liang, Y.; Hong, S.; Xia, C.; Wu, Y.; Li, J.; Cai, L.; Sonne, C.; Le, Q. V.; Lam, S. S. High capacity oil absorbent wood prepared through eco-friendly deep eutectic solvent delignification. *Chem. Eng. J.* **2020**, *401*, 126150. https://doi.org/10.1016/j.cej.2020.126150.

(28) Suopajärvi, T.; Ricci, P.; Karvonen, V.; Ottolina, G.; Liimatainen, H. Acidic and alkaline deep eutectic solvents in delignification and nanofibrillation of corn stalk, wheat straw, and rapeseed stem residues. *Ind. Crops Prod.* **2020**, *145*, 111956. https://doi.org/10.1016/j.indcrop.2019.111956.

(29) Sluiter, A. Determination of structural carbohydrates and lignin in biomass: Laboratory analytical procedure (LAP); Issue Date: April 2008; Revision Date: July 2011 (Version 07-08-2011). *Technical Report* **2008**, 18.

(30) Sarkanen, K. V.; Ludwig, C. H. *Lignins: occurrence, formation, structure and reactions*; Wiley-Interscience: New York, 1971.

(31) Willför, S.; Pranovich, A.; Tamminen, T.; Puls, J.; Laine, C.; Suurnäkki, A.; Saake, B.; Uotila, K.; Simolin, H.; Hemming, J.; Holmbom, B. Carbohydrate analysis of plant materials with uronic acid-containing polysaccharides–A comparison between different hydrolysis and subsequent chromatographic analytical techniques. *Ind. Crops Prod.* **2009**, *29* (2–3), 571–580. https://doi.org/10.1016/j.indcrop.2008.11.003.

(32) Barana, D.; Salanti, A.; Orlandi, M.; Ali, D. S.; Zoia, L. Biorefinery process for the simultaneous recovery of lignin, hemicelluloses, cellulose nanocrystals and silica from rice husk and arundo donax. *Ind. Crops Prod.* **2016**, *86*, 31–39. https://doi.org/10.1016/j.indcrop.2016.03.029.

(33) Brandt, A.; Chen, L.; van Dongen, B. E.; Welton, T.; Hallett, J. P. Structural changes in lignins isolated using an acidic ionic liquid water mixture. *Green Chem.* **2015**, *17* (11), 5019–5034. https://doi.org/10.1039/C5GC01314C.

(34) Wu, M.; Zhao, D.; Pang, J.; Zhang, X.; Li, M.; Xu, F.; Sun, R. Separation and characterization of lignin obtained by catalytic hydrothermal pretreatment of cotton stalk. *Ind. Crops Prod.* **2015**, *66*, 123–130. https://doi.org/10.1016/j.indcrop.2014.12.056.

(35) Adebisi, J. A.; Agunsoye, J. O.; Bello, S. A.; Kolawole, F. O.; Ramakokovhu, M. M.; Daramola, M. O.; Hassan, S. B. Extraction of silica from sugarcane bagasse, cassava reriderm and maize stalk: Proximate analysis and physico-chemical properties of wastes. *Waste Biomass Valor* **2019**, *10* (3), 617–629. https://doi.org/10.1007/s12649-017-0089-5.

(36) Kraszkiewicz, A.; Kachel-Jakubowska, M.; Niedziolka, I. The chemical composition of ash from the plant biomass in terms of indicators to assess slagging and pollution of surface heating equipment. *Fresenius Environ. Bull.* **2017**, *26* (11), 6383-6389.

(37) Li, R.; Kai, X.; Yang, T.; Sun, Y.; He, Y.; Shen, S. Release and transformation of alkali metals during co-combustion of coal and sulfur-rich wheat straw. *Energy Convers. Manage.* **2014**, *83*, 197–202. https://doi.org/10.1016/j.enconman.2014.02.059.

(38) Merdy, P.; Guillon, E.; Dumonceau, J.; Aplincourt, M. Characterisation of a wheat straw cell wall residue by various techniques: A comparative study with a synthetic and an extracted lignin.

Anal. Chim. Acta **2002***, 459,* 133–142. https://doi.org/10.1016/S0003-2670(02)00078-8

(39) Dorris, G.M.; Grey, D.G. The surface analysis of paper and wood fibers by ESCA I. Application to cellulosics and lignin. Cellul. Chem. Technol. **1978**, *12*, 9–23.

(40) Lange, H.; Schiffels, P.; Sette, M.; Sevastyanova, O.; Crestini, C. Fractional precipitation of wheat straw organosolv lignin: macroscopic properties and structural insights. *ACS Sustainable Chem. Eng.* **2016**, *4* (10), 5136–5151. https://doi.org/10.1021/acssuschemeng.6b01475.

(41) Myint, A. A.; Lee, H. W.; Seo, B.; Son, W.-S.; Yoon, J.; Yoon, T. J.; Park, H. J.; Yu, J.; Yoon, J.; Lee, Y.-W. One pot synthesis of environmentally friendly lignin nanoparticles with compressed liquid carbon dioxide as an antisolvent. *Green Chem.* **2016**, *18* (7), 2129–2146. https://doi.org/10.1039/C5GC02398J.

(42) Pan, X.-J.; Sano, Y. Comparison of acetic acid lignin with milled wood and alkaline lignins from wheat straw. *Holzforschung* **2000**, *54* (1), 61–65. https://doi.org/10.1515/HF.2000.009.

(43) Hong, S.; Lian, H.; Sun, X.; Pan, D.; Carranza, A.; Pojman, J. A.; Mota-Morales, J. D. Zinc-based deep eutectic solvent-mediated hydroxylation and demethoxylation of lignin for the production of wood adhesive. *RSC Adv.* **2016**, *6* (92), 89599–89608. https://doi.org/10.1039/C6RA18290A.

(44) Shen, D. K.; Gu, S.; Luo, K. H.; Wang, S. R.; Fang, M. X. The pyrolytic degradation of wood-derived lignin from pulping process. *Bioresour. Technol.* **2010**, *101* (15), 6136–6146. https://doi.org/10.1016/j.biortech.2010.02.078.

(45) Tejado, A.; Peña, C.; Labidi, J.; Echeverria, J. M.; Mondragon, I. Physico-chemical characterization of lignins from different sources for use in phenol–formaldehyde resin synthesis. *Bioresour. Technol.* **2007**, *98* (8), 1655–1663. https://doi.org/10.1016/j.biortech.2006.05.042.

(46) Imai, T.; Yokoyama, T.; Matsumoto, Y. Revisiting the mechanism of β-O-4 bond cleavage during acidolysis of lignin: Part 5: On the characteristics of acidolysis using hydrobromic acid. *J. Wood Chem. Technol.* **2012**, *32* (2), 165–174. https://doi.org/10.1080/02773813.2011.624668.

(47) Imai, T.; Yokoyama, T.; Matsumoto, Y. Revisiting the mechanism of β-O-4 bond cleavage during acidolysis of lignin IV: Dependence of acidolysis reaction on the type of acid. *J. Wood Chem. Technol.* **2011**, *57* (3), 219–225. https://doi.org/10.1007/s10086-010-1166-6.

(48) Yokoyama, T.; Matsumoto, Y. Revisiting the mechanism of β-O-4 bond cleavage during acidolysis of lignin. Part 2: Detailed reaction mechanism of a non-phenolic C_6-C_2 type model compound. *J. Wood Chem. Technol.* **2010**, *30* (3), 269–282. https://doi.org/10.1080/02773811003675288.

(49) Yokoyama, T.; Matsumoto, Y. Revisiting the mechanism of β-O-4 bond cleavage during acidolysis of lignin. Part 1: Kinetics of the formation of enol ether from non-phenolic C_6-C_2 type model compounds. *Holzforschung* **2008**, *62* (2), 164–168. https://doi.org/10.1515/HF.2008.037.

Table and Figure Captions

Table 1. The chemical composition and purity of lignins from alkaline and acidic DES treatments (KGL and LCL, respectively).

Table 2. Elemental compositions of KGL and LCL determined by elemental analysis and XPS analysis.

Table 3. The functional groups of KGL and LCL classified on the basis of the C 1s and O 1s peaks.

Table 4. Weight-average (Mw) and number-average (Mn) molecular weight and the polydispersity index (PDI) of KGL and LCL.

Table 5. Quantitative ^{13}C and ^{31}P NMR analysis of KGL and LCL.

Figure 1. Core-level XPS spectra C 1s and O 1s for KGL and LCL.

Figure 2. Molecular weight (a) and particle size distributions (b) of KGL and LCL.

Figure 3. FESEM (a–d) and TEM images (e–f) of KGL (left) and of LCL (right). Scale bar at upper row is 2 μm, in the middle 200 nm, and at the bottom row 500 nm.

Figure 4. TG-DTG curves (a) and DRIFT spectra (b) of KGL, LCL and wheat straw (WS).

Figure 5. ^{13}C NMR spectra of KGL and LCL.

Figure 6. ^{31}P NMR of KGL and LCL. (a) The full region of interest of the lignin KGL. (b) The full region of interest of the lignin LCL. The integration regions are highlighted by blue dashed lines. (c) Deconvoluted spectrum of an overlapping region of KGL lignin. (d) Deconvoluted spectrum of an overlapping region of LCL lignin. In the deconvoluted spectra, the black solid line corresponds to the experimental spectra, the blue dotted corresponds to the deconvoluted peaks, and the red dashed line corresponds to the sum of the deconvoluted peaks. Some peaks are cut (~) to illustrate the features better.

Figure 7. HSQC NMR spectra of KGL and LCL.

Table 1. The chemical composition and purity of lignins from alkaline and acidic DES treatments (KGL and LCL, respectively).

	DES-lignin samples	
	KGL	LCL
AIL [%]	73.0 ± 2.0	82.3 ± 1.3
ASL [%]	1.8 ± 0.1	1.2 ± 0.1
Ash [%]	15.0 ± 0.4	0.7 ± 0.2
Lignin purity[a] [%]	74.8	83.5
Lignin yield[b] [%]	7.8 ± 0.6	6.1 ± 0.6
D-Glucose [%]	0.65 ± 0.01	0.77 ± 0.01
D-Xylose [%]	1.14 ± 0.02	1.02 ± 0.01
L-Arabinose [%]	0.67 ± 0.01	0.75 ± 0.05
L-Galactose [%]	0.52 ± 0.01	<0.10
D-Mannose [%]	0.1 ± 0.00	<0.10
Carbohydrates[c] [%]	3.3	2.9
Polysaccharides[d] [%]	2.9	2.6

[a] Lignin purity was calculated from the sum of AIL (%) and ASL (%).
[b] Yields of lignin samples were based on the weight of the oven-dried wheat straw (obtained lignin/original biomass).
[c] Total yield of monosaccharides.
[d] Calculated from the corresponding monosaccharides.

Table 2. Elemental compositions of KGL and LCL determined by elemental analysis and XPS analysis.

DES-lignin samples	C	H	O	N	S	Si	O/C	Total
KGL								
(Elemental analysis) [%]	50.20 ± 0.49	5.70 ± 0.08	22.60 ± 0.39	1.10 ± 0.01	< 0.10	—	—	79.6
(XPS) [atomic %]	62.47	1.18	28.75	—	—	7.59	0.46	—
LCL								
(Elemental analysis) [%]	60.80 ± 0.20	6.10 ± 0.02	29.60 ± 2.10	1.60 ± 0.01	< 0.10	—	—	98.1
(XPS) [atomic %]	73.38	1.7	24.75	—	—	0.17	0.34	—

Table 3. The functional groups of KGL and LCL classified on the basis of C 1s and O 1s peaks.

DES-lignin Samples	Relative content of each linkage peak					
	C 1s (%)			O 1s (%)		
	C_1[a] (284.8 eV)	C_2[b] (286.32 eV)	C_3[c] (287.45 eV)	O_1[d] (531.75 eV)	O_2[e] (532.7 eV)	O_3[f] (533.16 eV)
KGL	77.15	15	7.86	4.76	9.22	86.01
LCL	60.62	34.41	4.97	19.81	10.55	69.64

[a] C−C or C−H linkages
[b] C−O−C and C−OH linkages
[c] O=C−OH linkages
[d] Ph=O, Ph−C=O, and O−O linkages
[e] C=O and O=C−OH linkages
[f] Ph−OH and C−O linkages

704 **Table 4.** Weight-average (Mw) and number-average (Mn) molecular weight and the
705 polydispersity index (PDI) of KGL and LCL.

DES-lignin samples	Mw (g/mol)	Mn (g/mol)	PDI (Mw/Mn)
KGL	5696	1396	4.08
LCL	3215	1042	3.09
MWL[a]	3570	1970	1.81
Alkaline lignin[a]	3270	1770	1.85
Acetic acid lignin[a]	4430	2020	2.19

706 [a] Reported in literature[41].

707

Table 5. Quantitative ^{13}C and ^{31}P NMR analysis of KGL and LCL.

NMR spectra	Spectral region	Chemical shift (ppm)	Content[a]	
			KGL	LCL
^{13}C NMR	CH_3O	57-54	1.62	1.83
	C_{Ar}-H	125-103	2.26	2.66
	C_{Ar}-C	141-125	1.60	1.61
	C_{Ar}-O	160-141	2.14	1.73
	Aliphatic side chain	34-12	3.09	2.26
	Cγ in β-5 and β-O-4 with C=O	64-62	0.34	0.61
	Cα in β-O-4	78-71	0.79	Trace
	Cβ in β-O-4	83-78	0.30	Trace
^{31}P NMR	Aliphatic OH	149.0-144.7	2.00	1.94
	Syringyl OH (S-units)	142.8-140.6	0.54	0.52
	C_5 substituted and guaiacyl OH (5-sub. and G-units)	140.5-137.5	0.84	0.79
	p-Hydroxyphenyl OH (H-units)	137.5-136.0	0.19	0.49
	Tricin	136.0-134.7	0.11	0.24
	Carboxylic OH	134.7-132.7	0.46	0.45
	Total phenolic OH[b]	142.8-136.0	1.57	1.80

[a] Units: ^{13}C NMR: moieties per Ar, ^{31}P NMR: mmol/g lignin.

[b] The total content of phenolic hydroxyl group (i.e., guaiacyl, syringyl, C_5-substituted guaiacyl phenolics, *p*-hydroxyphenols)

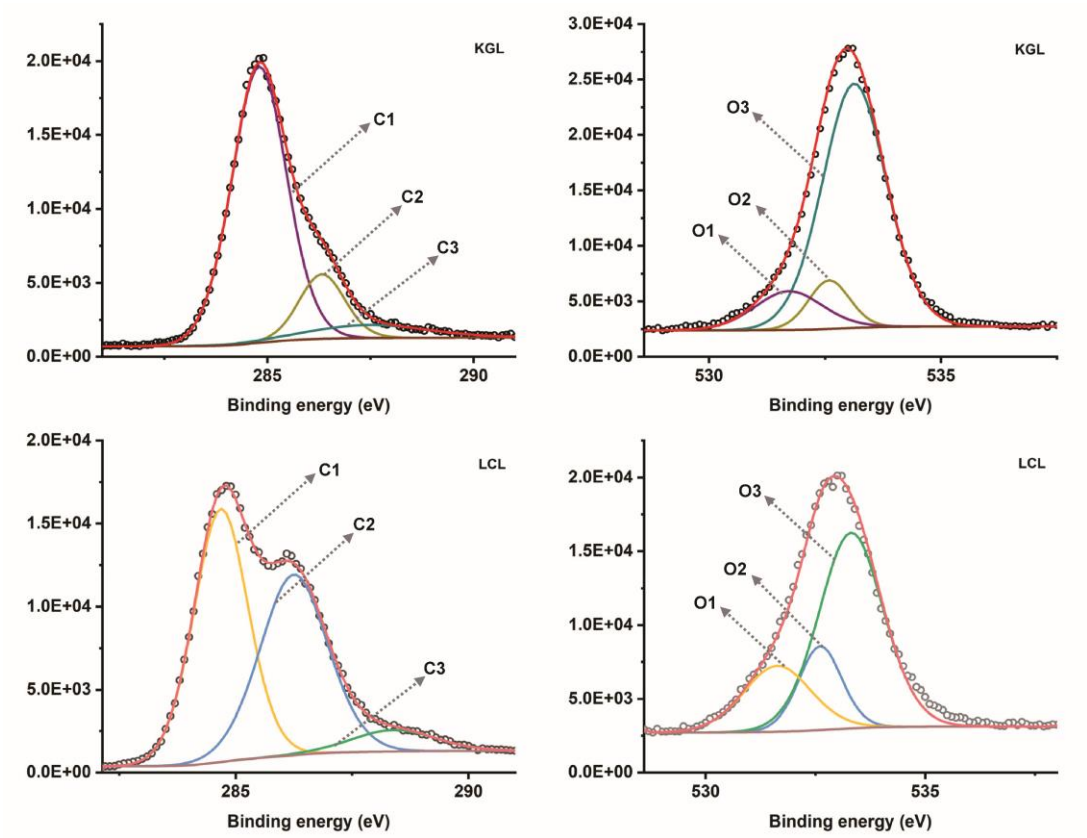

Figure 1. Core-level XPS spectra C 1s and O 1s for KGL and LCL.

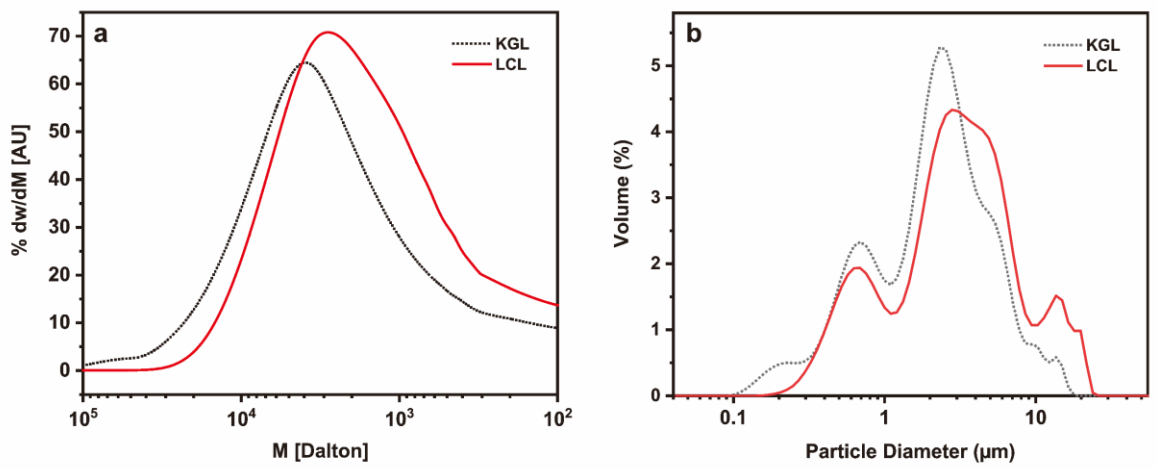

716

717 **Figure 2.** Molecular weight (a) and particle size distributions (b) of KGL and LCL.

718

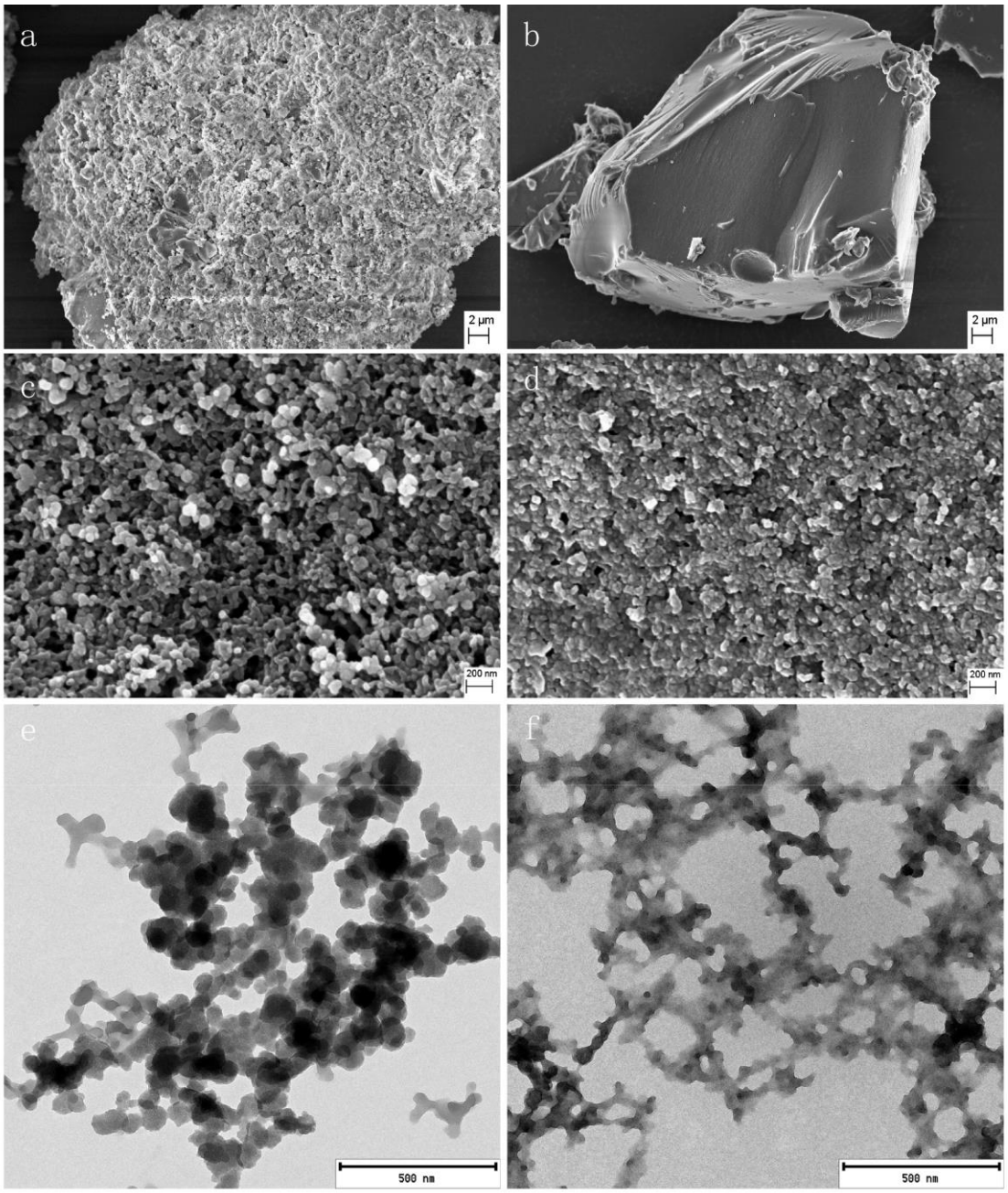

Figure 3. FESEM (a–d) and TEM images (e–f) of KGL (left) and of LCL (right). Scale bar at upper row is 2 µm, in the middle 200 nm, and at the bottom row 500 nm.

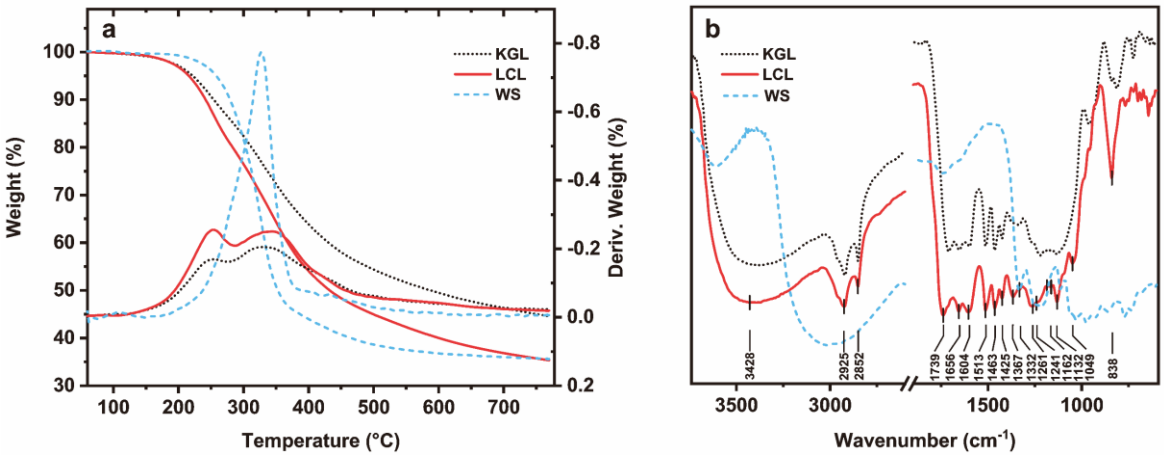

Figure 4. TG-DTG curves (a) and DRIFT spectra (b) of KGL, LCL and wheat straw (WS).

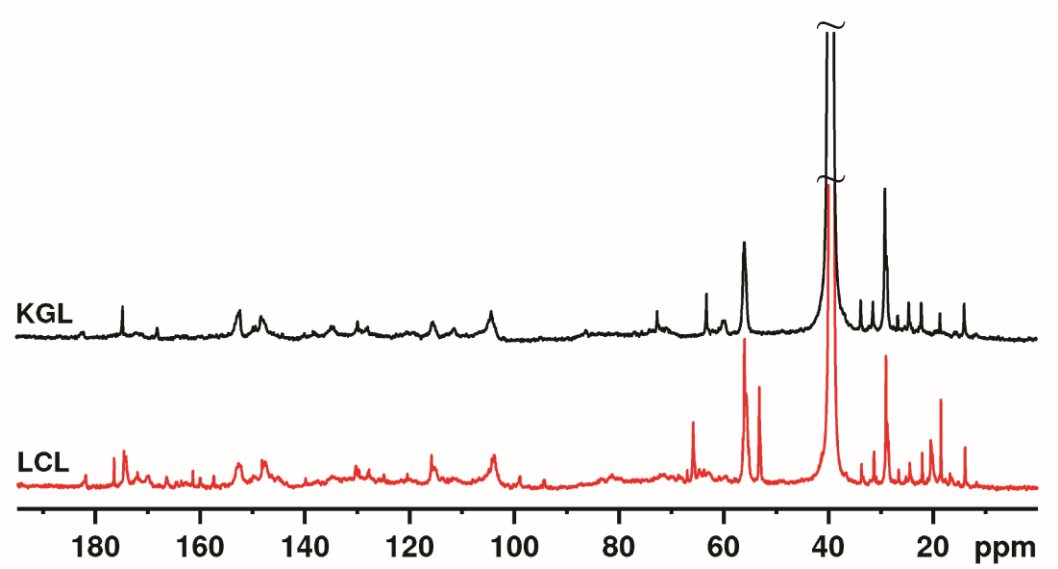

Figure 5. ^{13}C NMR spectra of KGL and LCL.

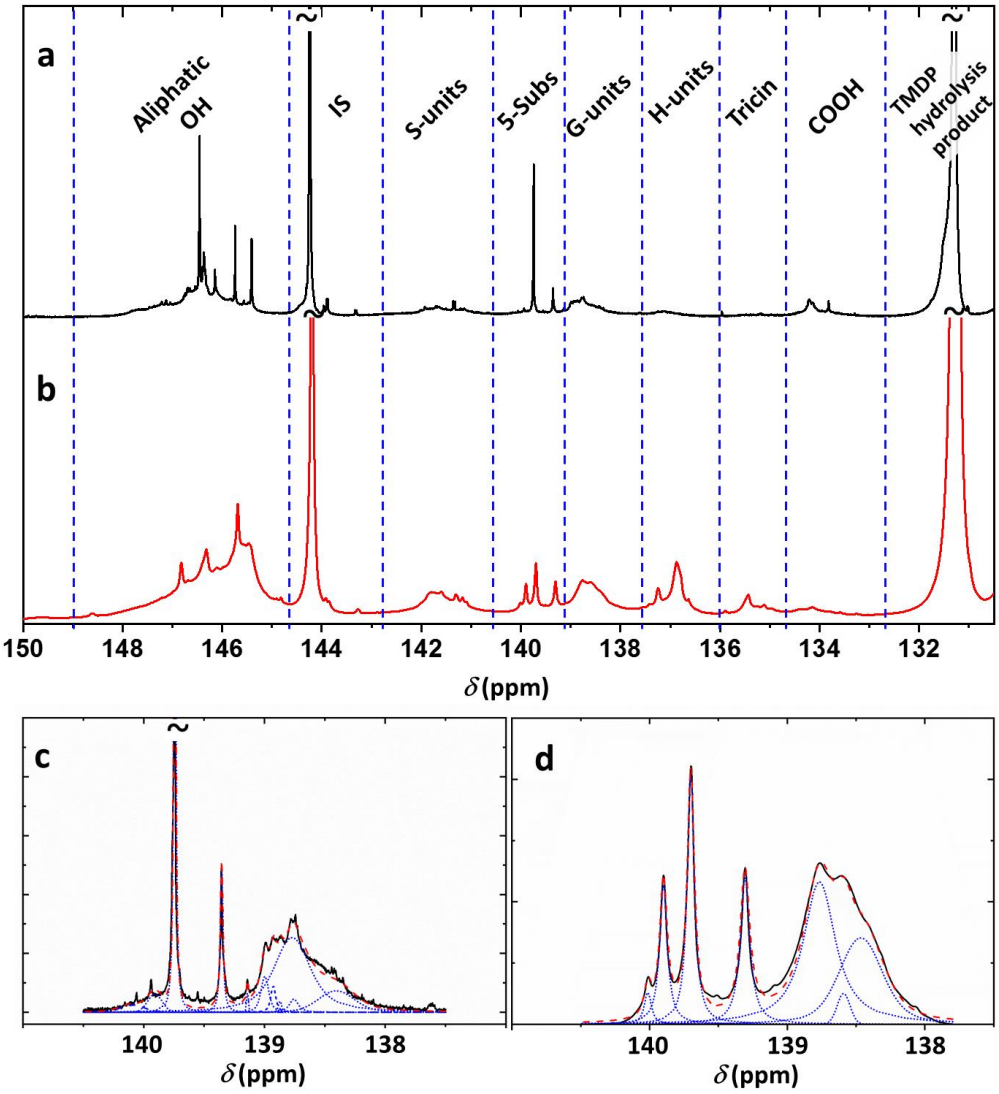

Figure 6. ^{31}P NMR of KGL and LCL. (a) The full region of interest of the lignin KGL. (b) The full region of interest of the lignin LCL. The integration regions are highlighted by blue dashed lines. (c) Deconvoluted spectrum of an overlapping region of KGL lignin. (d) Deconvoluted spectrum of an overlapping region of LCL lignin. In the deconvoluted spectra, the black solid line corresponds to the experimental spectra, the blue dotted corresponds to the deconvoluted peaks, and the red dashed line corresponds to the sum of the deconvoluted peaks. Some peaks are cut (~) to illustrate the features better.

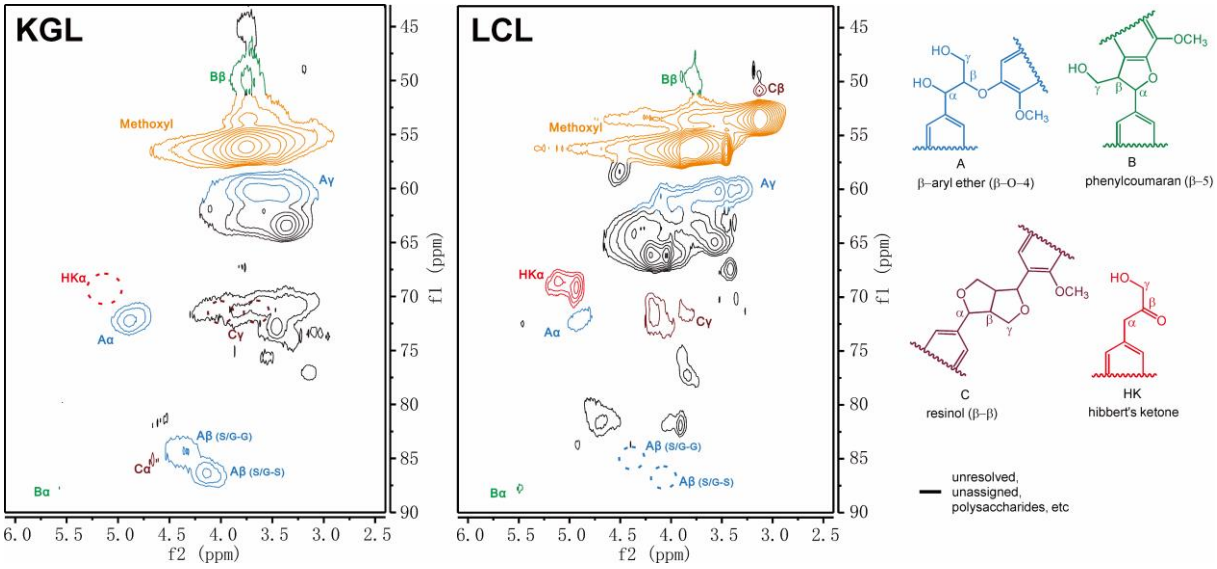

Figure 7. HSQC NMR spectra of KGL and LCL.

742 **Table of contents graphic image:**

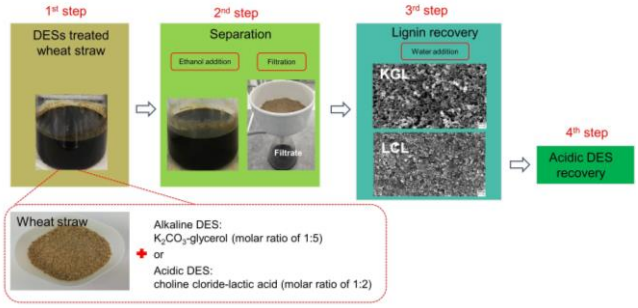

743